Ultramicroscopy ■ (■■■■) ■■■–■■■

Contents lists available at ScienceDirect

Ultramicroscopy

journal homepage: www.elsevier.com/locate/ultramic

Removing the effects of the "dark matter" in tomography

Lionel C. Gontard

Instituto de Ciencia de Materiales de Sevilla (CSIC), 41092 Sevilla, Spain

ARTICLE INFO

Article history:
Received 16 October 2014
Received in revised form
10 March 2015
Accepted 18 March 2015

Keywords:
Tomography
Electron tomography
Tilt series
Image processing

ABSTRACT

Electron tomography (ET) using different imaging modes has been progressively consolidating its position as a key tool in materials science. The fidelity of a tomographic reconstruction, or tomogram, is affected by several experimental factors. Most often, an unrealistic cloud of intensity that does not correspond to a real material phase of the specimen ("dark matter") blurs the tomograms and enhances artefacts arising from the missing wedge (MW). Here we show that by simple preprocessing of the background level of any tomographic tilt series, it is possible to minimise the negative effects of that "dark matter". Iterative reconstruction algorithms converge better, leading to tomograms with fewer streaking artefacts from the MW, more contrast, and increased accuracy. The conclusions are valid irrespective of the imaging mode used, and the methodology improves the segmentation and visualisation of tomograms of both crystalline and amorphous materials. We show examples of HAADF STEM and BF TEM tomography.

1. Introduction

Electron tomography (ET) in materials science is a technique based on the acquisition of a series of projected images from a sample by tilting the specimen using a microscope goniometer and can be combined with spectroscopic data [1–4]. It provides important 3D structural and chemical information that makes it possible to correlate the synthesis, structure, and functionality of a diversity of nanostructures even at atomic resolution [5–16]. ET application follows a series of steps (Fig. 1a). In transmission electron microscopy (TEM), usually 'single-axis tilting' is used, in which the specimen is tilted about the eucentric axis of the specimen holder rod. After accurate alignment of the tomographic tilt series, reconstruction, segmentation, and visualisation of the 3D volume or tomogram are the steps necessary to extract quantitative morphological information from the 3D tomograms [17–20].

For optimal results, the specimen must be tilted over a tilt that is as close to $\pm 90°$ as possible, but in practise the maximum tilting range rarely exceeds $\pm 75°$. This is the well-known problem of the missing wedge (MW) of information that results in a decrease of the spatial resolution and the presence of artefacts in the tomogram [1–4]. For certain types of sample geometries, the use of double-tilting, full-rotation holders and adapted preparation methods can be used for decreasing the MW [21,22]. Important progress in ET has resulted from digital processing of tomographic tilt series before 3D reconstruction by accurate interpolation of sinograms, edge detection, contrast enhancement, and accurate alignment of tilt series [23–26]. The next step is the reconstruction of the tomogram, typically using weighted back-projection (WP) or the simultaneous iterative reconstruction technique (SIRT) [3,24]. Nonetheless, much effort is being put into novel reconstruction algorithms which can notably improve the quality of tomograms, even with low sampling and limited angular range, using either the discretisation of intensities, the calculation of sinusoidal trajectories in sinograms, the incorporation of geometric prior knowledge, or compressive sensing [27–31]. Tomograms obtained after the reconstruction are 3D datasets containing a continuous range of intensity levels, and therefore in order to extract useful information, visualisation and segmentation are required in combination with the application of sophisticated algorithms, such as anisotropic non-linear diffusion, to reduce noise and enhance local structure without worsening the resolution or structural information, adaptive thresholding, or equalisation in real space [32–35]. In the present work, we focus on the effects of an experimental parameter: the minimum value of the intensity used to acquire a tomographic tilt series. Our results show that by optimisation of the background level of a tomographic tilt series it is possible to dramatically improve the quality of the tomogram.

2. Methods

In our experiments we use a commercial software package for acquisition and reconstruction of tomographic tilt series called *Explore3D*, which is the standard for TEMs manufactured by FEI.

E-mail address: lionelcg@gmail.com

http://dx.doi.org/10.1016/j.ultramic.2015.03.017
0304-3991/

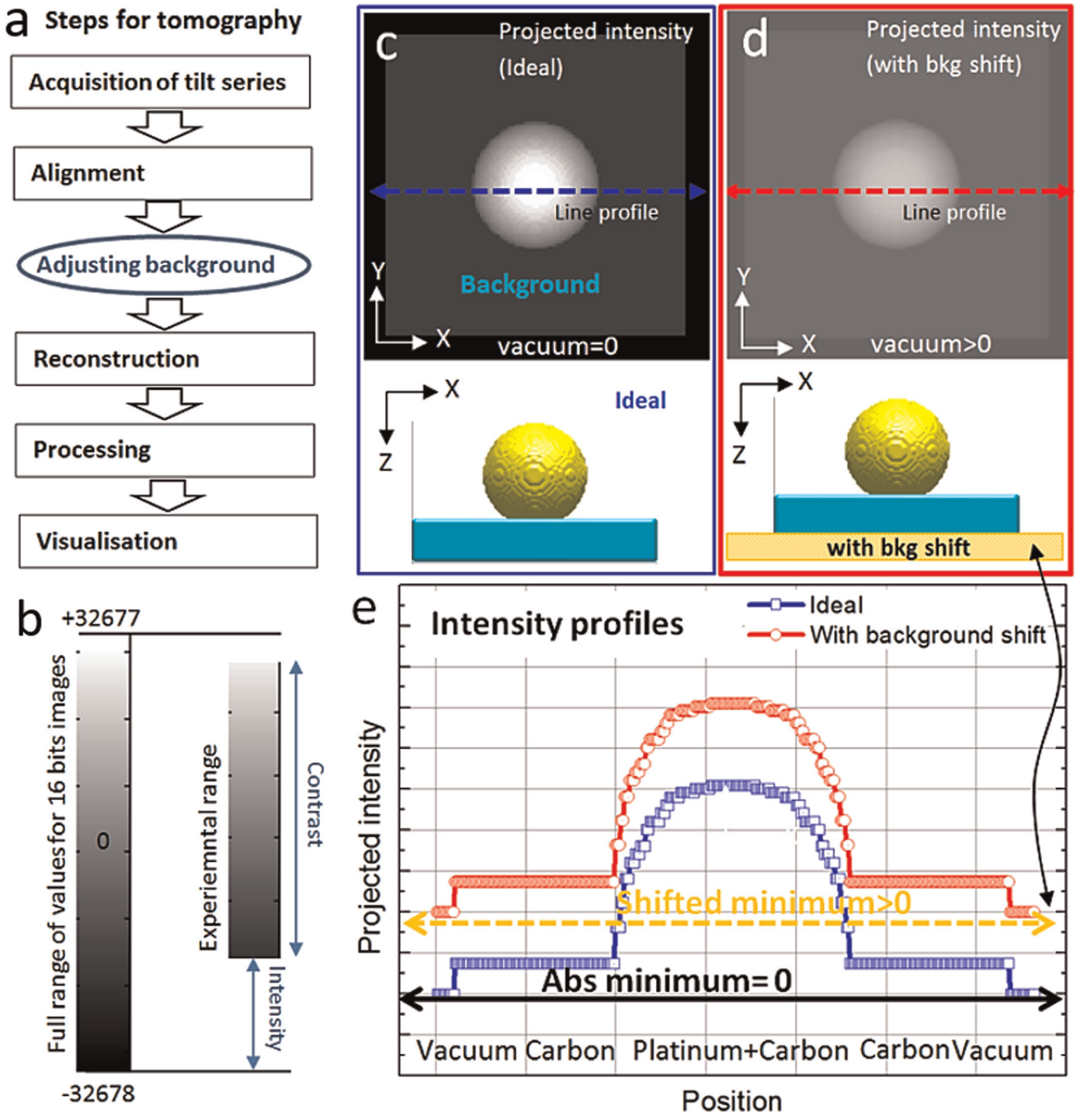

Fig. 1. Tomographic tilt series and minimum intensity. (a) Typical steps performed in electron tomography. A step consisting in the optimisation of the background level of a tilt series is required before reconstruction. (b) Difference between the bit resolution of the detector and the range of intensities used while adjusting I/C. (c and d) Model of one spherical Pt particle supported on a C film surrounded by vacuum and the corresponding projected intensity images with and without background shift. (e) Intensity profiles measured along the arrowed lines shown in (c) and (d). In the ideal situation, the vacuum level coincides with the absolute minimum value of the recording system (blue curve with squares). In practise the images of a tilt series are often recorded with a different minimum (red curve with circles). The shift is equivalent to the presence of a layer of material that does not exist. (For interpretation of the references to colour in this figure legend, the reader is referred to the web version of this article.)

The file format is a version of the original one.mrc created by the Medical Research Council..With this software, the pixel intensities of the tilt series of images are recorded as numbers with the format of *integer signed* and 16 bits, meaning that pixels can take discrete values in the range between −32,678 and +32,677. In order to optimise the background of the tilt series, the minimum value of the matrix I_{min} is found and the values of the matrix are downshifted by an amount given by the difference between −32,678 and I_{min}. The resulting matrix is saved back into the FEI format for subsequent tomographic reconstruction.

It is worth mentioning here that the basis of tomography, the Radon transform defines a projection function (an image in TEM) as an integral from zero. Similarly, in order to converge to a correct solution iterative reconstruction methods require the values of intensities to be positive, i.e., that the intensities must be equal or above zero [36]. Because the software of FEI reconstructs

tomographic series correctly we assume here that the range of signed values used in the FEI software is only for storage and visualisation purposes, and that the reconstruction algorithms must rescale internally the intensities so that they are unsigned for reconstruction purposes.

The tomographic HAADF STEM series shown in Fig. 3 was obtained using a Tecnai F30 with a field-emission gun (FEGTEM) operated at 200 kV. Images in Fig. 4 were acquired using an aberration-corrected Titan TEM (FEGTEM) operated at 300 kV and a camera length corresponding to inner detector semi-angles of ≈ 90 mrad to enhance the contrast between the cores and the shells of the particles while minimising diffraction. Images were acquired using a single-tilt tomography holder model 2020 (from Fischione Instruments). Alignment and tomographic reconstruction of the tilt series were performed using the SIRT algorithm with 15 iterations using Inspect3D software from FEI. The same software was used to invert the contrast of the BF TEM series of Fig. 5. Visualisation using voltex and orthoslices, segmentation, isosurface rendering, and Sobel filtering of the 3D datasets was performed using Avizo software. The tomographic BF TEM series shown in Figs. 5 and 6 was acquired using the same Titan microscope and a CCD camera. Image contrast is defined as

$$C = I_{max} - I_{min}/I_{max} + I_{min}$$

For the optimisation of the background of the tilt series and algorithm was implemented using Matlab. An aligned tilt series of images is loaded into a matrix. The matrix contains the intensities of every pixel of the tomographic series. The intensities that form an image as measured by a detector system must be transformed into the digital domain by analogue-to-digital conversion so that pixel intensities that are recorded in an image take discrete values within a range that depends on the bit resolution of the detector system.

3. Intensity of a tilt series and background optimisation

When an experimental tomographic tilt series of images is acquired during an experiment, it is necessary to first adjust the minimum value and the range of values of pixel intensities acquired by a detector by varying the Offset and Gain (O/G) parameters (which correspond with the imaging parameters intensity and contrast). Normally, the adjustment of O/G is done by checking that the image is correctly recorded at a finite number of tilts (e.g. 0°, ±30°, ±70°). Nevertheless, because an useful tilt series requires the acquisition of many more images (typically with a tilt step of 2°), the O/G adjustment made for some images may not be valid for the whole series of images because there will be thickness changes and variations in diffraction contrast that cannot be controlled a priori. If the experiment is performed such that the *intensity* level is too low or if the *contrast* range is too wide, the pixel intensities of some images can fall outside the dynamic range of the detector, and parts of the images will become oversaturated or will be undersaturated at several tilts.

Therefore it is a common practise to adjust the O/G *level within a range of values that is narrower than the full available bit resolution of the detector* (or of the image format used for storing the images) (see Fig. 1b). The drawback of this strategy is that the background level of *every* image of the experimental tilt series will be shifted by an indefinite constant towards higher values of intensity. This is certainly the case for most specimens when there is not available a vacuum region to define a zero reference level of intensity. On the other hand, most often when performing ET of a nanostructure, we are not interested in its surrounding (the supporting film or a containing matrix). Hence, we propose here to minimise the background level of intensity of the images of a tilt series at the expense of *not* reconstructing the space surrounding de nanostructure. Such step eliminates the uncertainty of lacking for a reference level of intensity while it improves the fidelity of the reconstruction of the nanostructure of interest.

Fig. 1c and d shows a simulated HAADF STEM image (representative of one image of a tomographic tilt series) of a model of a high-density spherical particle suspended on a lower density film and surrounded by vacuum. Intensities can take values between 0 (black) and 1 (white). In Fig. 1c the minimum intensity (that of vacuum) coincides with 0, the minimum value available with a hypothetical detector system. In Fig. 1d the minimum intensity (that of vacuum) is shifted to a value >0. Fig. 1e shows the intensity profiles along the centre of the images in Fig. 1c and d. The background shift (see dashed orange line) is equivalent to adding new material that is not real (orange colour in Fig. 1d) to the model of the specimen. But if a tilt series of images such the one in Fig. 1d is used for tomographic reconstruction, the orange layer will show up in the tomogram as a real material that will introduce artefacts. It is known that if a carbon film used as support for tomography is thick, then it can introduce artefacts in a reconstruction such as the top–bottom effect [37].

However, the problem described in this paper is a worse situation because the *orange layer in Fig. 1d is present in every image of the tilt series, as a thick layer that is not limited in space and it will show up in every voxel (3D pixel) of the tomogram.* Fig. 2a–c compares the tomographic reconstruction of an object model (a "phantom") shown in Fig. 2a with a more realistic reconstruction with a MW of 40° and using projections of the "phantom" with and without background shift (Fig. 2b and c respectively). Fig. 2d shows three intensity profiles along the central lines of the "phantoms". It is clear that in the case of using a tilt series without a shift of the background level (blue line, $I_{min} \approx 0$) the contrast of the reconstruction increases, the intensities quantitatively match the intensity range of the original "phantom" more accurately, and there are fewer artefacts outside the phantom. In summary, if an inappropriate background level above zero is chosen an artificial extra thickness is added to the support of the sample in the experimental tomographic tilt series.

4. Experimental results

4.1. HAADF STEM tomography: Improving contrast and reducing artefacts

Fig. 3a is an experimental image acquired at 0° representative of a HAADF STEM tilt series of a sample of $BiPO_4$ star-like particles [38]. The tilt series was acquired with a minimum intensity value of −619. This value is shifted by a large amount with respect to the absolute minimum value allowed by the detector system, that is, −32,768 for 16-bit resolution. The same tilt series was processed offline and its background level was downshifted by subtracting a constant value of +32,016 from every image (the difference between −32,678 and −619). Fig. 3b shows the central line profiles of intensities measured on the images at 0° tilt of the two tilt series with and without background optimisation. Tomograms were reconstructed from both tilt series and their histograms calculated (Fig. 3c). Both histograms display a maximum peak of counts at low intensities. These peaks correspond with voxels (3D pixels) that surround the particle. The histogram of the original tilt series (with an upwards background shift at −619) contains counts at intensities to the left of the maximum peak. So voxels of vacuum around the particle in are non-zero in the tomogram and blur the particle in Fig. 3d. In contrast, in Fig. 3e the contrast of the tomogram is much higher, and blurring around the particle

Please cite this article as: L.C. Gontard, Removing the effects of the "dark matter" in tomography, Ultramicroscopy (2015), http://dx.doi.org/10.1016/j.ultramic.2015.03.017

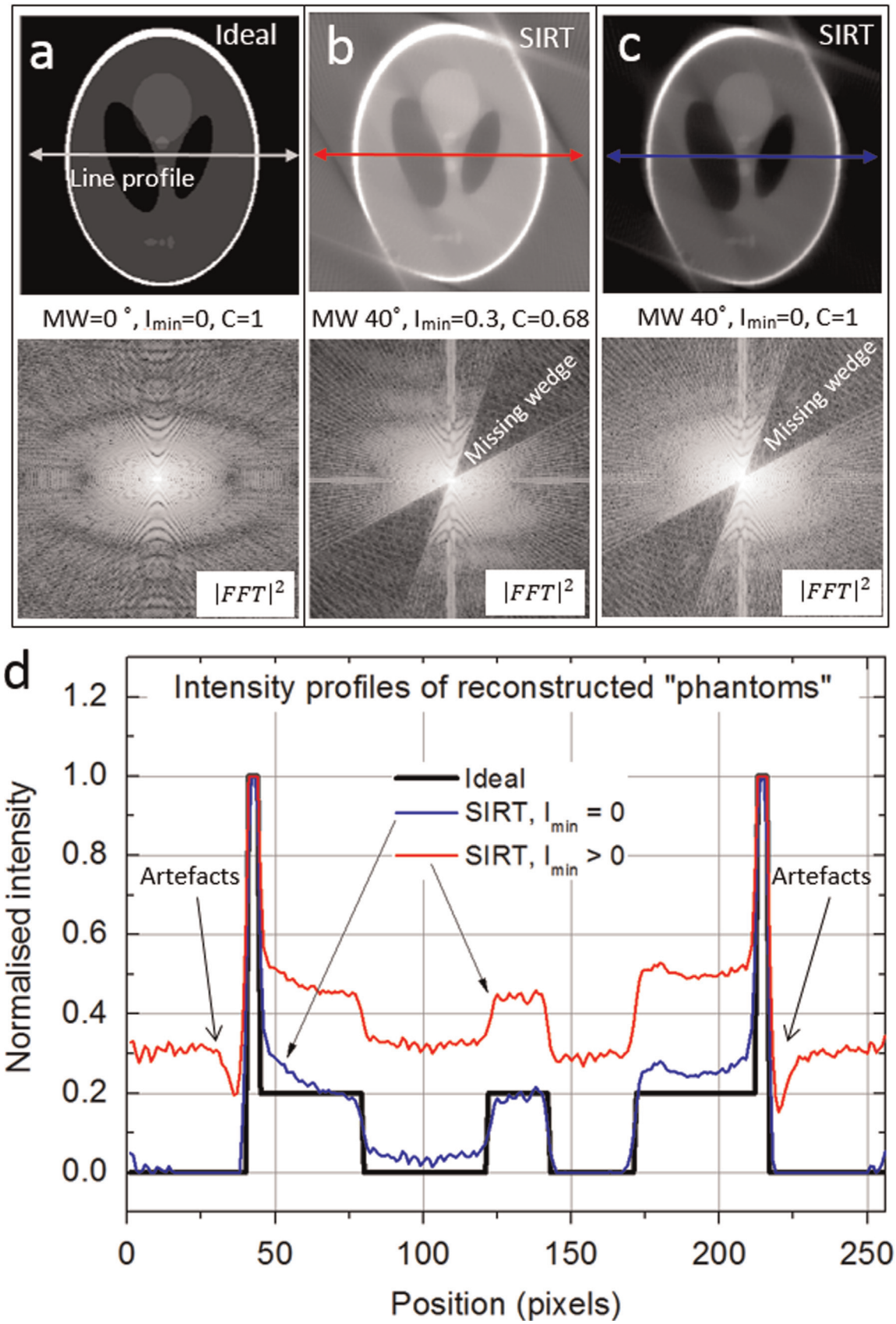

Fig. 2. SIRT reconstruction and background intensity. (a) Model of "phantom" that would be computed in an ideal tomographic experiment without MW. The full intensity range is [0, 1]. The background level is zero ($I_{min}=0$), and the contrast of the tomogram is $C=1$. (b) Simulation of a reconstructed "phantom" with a MW of 40° and tilt step of 2° using SIRT with 50 iterations. I_{min} of the tilt series shifted to 0.3. The contrast of the tomogram is now $C=0.63$. (c) Reconstructed "phantom" under the same conditions whereby (c) and the I_{min} of the tilt series are set exactly to zero. The contrast of the tomogram is 1 and artefacts outside the phantom are minimised. Below the tomograms, the corresponding diffractograms are shown. (d) Line profiles of the intensity of the tomograms (b) and (c) compared to the ideal case (a).

Please cite this article as: L.C. Gontard, Removing the effects of the "dark matter" in tomography, Ultramicroscopy (2015), http://dx.doi.org/10.1016/j.ultramic.2015.03.017

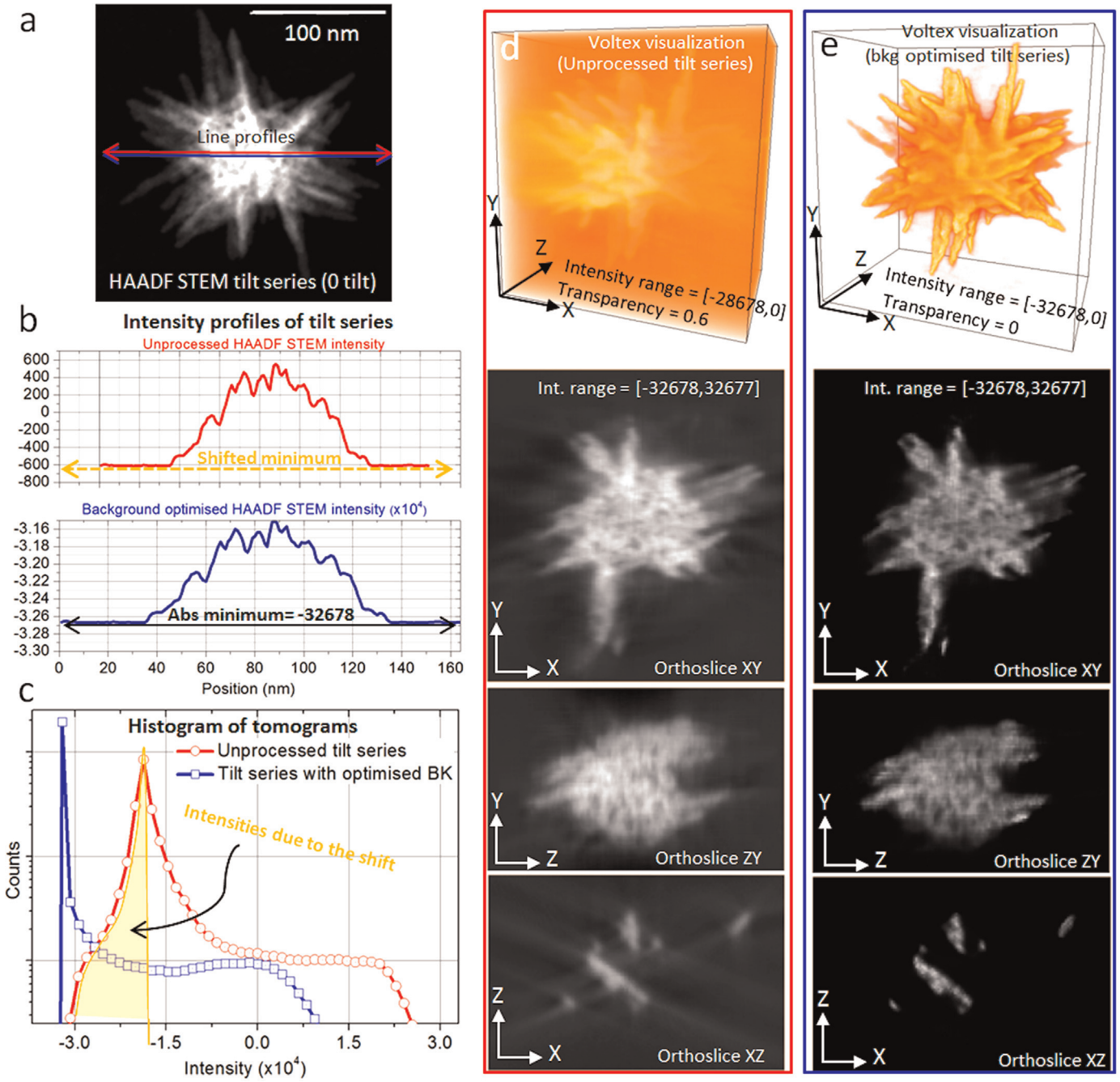

Fig. 3. Improving contrast and reduction of artefacts. a HAADF STEM image at 0° tilt representative of a tilt series of images of a $BiPO_4$ star-like particle acquired at 300 keV with a range of tilts between −70° and +70° (high tilt step of 1° above 60° and 2° tilt step below 60°). (b) The minimum intensity level recorded was at −619. After optimising the intensities, it was set to −32,635. (c) Histograms of the reconstructed tomograms before (in red and circles) and after background optimisation (in blue and squares). The histogram of the unprocessed series has intensity values to the left of the maximum peak (area in orange under the red curve) that blur the tomogram. (d) and (e) show the voltex visualisation and three orthogonal central sections of the tomograms. If the background of the tilt series is shifted, the tomogram will be surrounded by a cloud of intensity that does not correspond to real material ("dark matter") (Video S3 supporting info). (For interpretation of the references to colour in this figure legend, the reader is referred to the web version of this article.)

disappears. Moreover, streaking artefacts characteristic of the MW have almost disappeared, as shown in the orthoslices in Fig. 3d and e. Note that the orthoslices were not manipulated and they are displayed with the full dynamic range [−32,678, 32,677].

4.2. HAADF STEM tomography: improvement of segmentation

Blurring and artefacts in tomograms make their processing for visualisation and accurate segmentation difficult, leading to a requirement for dedicated human intervention that is subjective and time-consuming [17,19,25,35,39]. Fig. 4 shows an example of the improvement that can be obtained in the process of segmenting a tomogram when the background of the tilt series is optimised. The sample consist of bimetallic Au@Ag core–shell nanoparticles, used as tags in biorecognition, that were deposited on a thin carbon support for their investigation using HAADF STEM [40]. When the background is optimised (with a value close to −32,678), the edges and surfaces of the particles are much better defined (see orthoslices in Fig. 4c). Fig. 4d shows the same orthoslices after application of Sobel filtering, which is a common image-

Please cite this article as: L.C. Gontard, Removing the effects of the "dark matter" in tomography, Ultramicroscopy (2015), http://dx.doi.org/10.1016/j.ultramic.2015.03.017

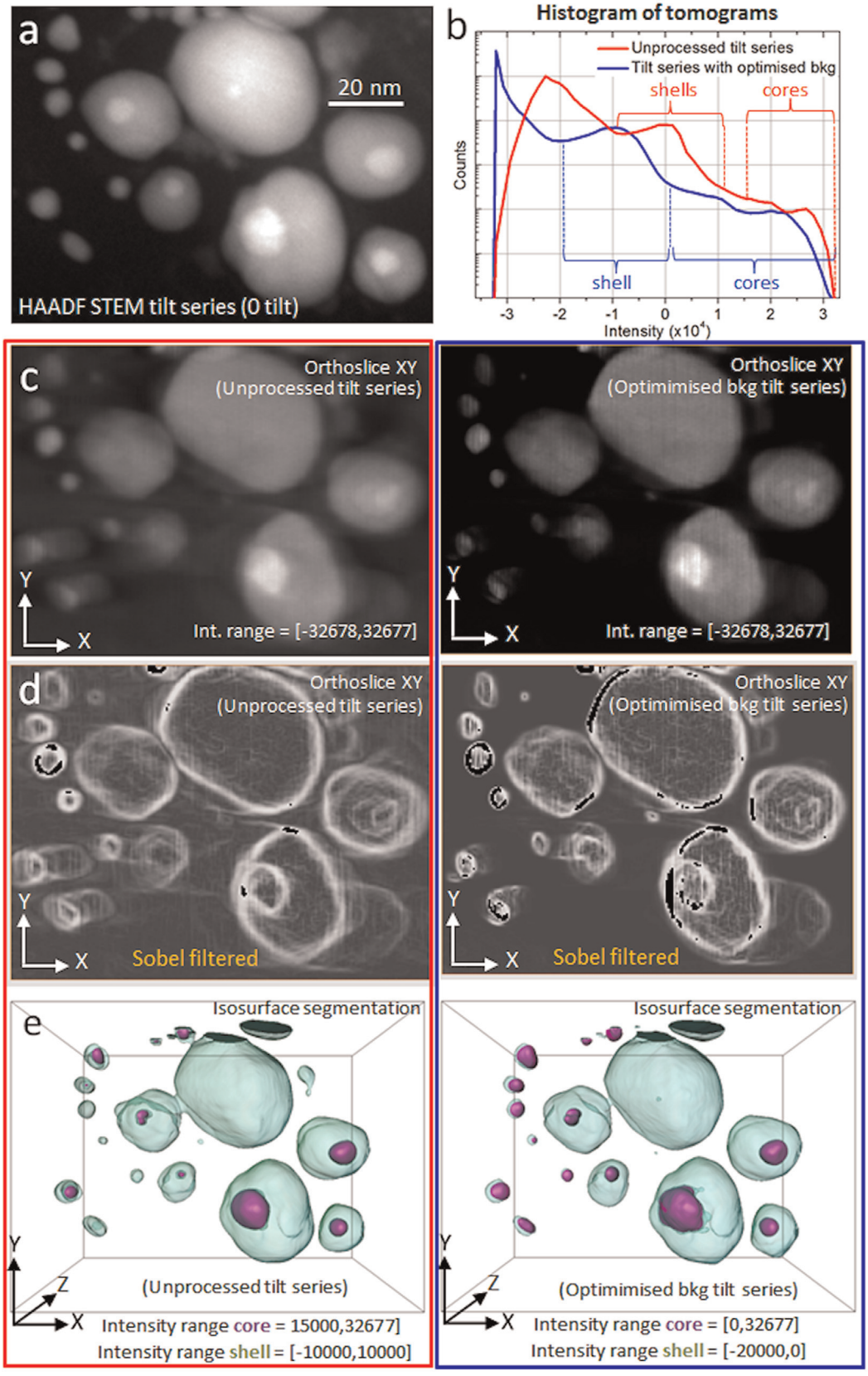

Fig. 4. Improvement of segmentation of tomograms. (a) HAADF STEM image at 0° tilt representative of a tilt series of 39 images of bimetallic Au/Ag core–shell nanoparticles with a tilt range from −60° to +70°, a high tilt step of 2°, and a low tilt step of 4° in steps with a tilt switch at 50°. (b) Histograms of the tomograms using the original tilt series (red) and the one with background optimisation (blue). (c) XY orthoslice of the tomogram obtained using the unprocessed tilt series (left) or the one with background optimisation (right). The contrast is enhanced and blurring disappears. (d) The same as in (c) after application of a Sobel filter. (e) Segmentation of the tomograms using the ranges of intensities in brackets shown in (a). (Video S2 supporting info). (For interpretation of the references to colour in this figure legend, the reader is referred to the web version of this article.)

Please cite this article as: L.C. Gontard, Removing the effects of the "dark matter" in tomography, Ultramicroscopy (2015), http://dx.doi.org/10.1016/j.ultramic.2015.03.017

processing operator used in edge detection algorithms that emphasises transitions of intensity maps by calculating local gradients. It is evident that there is an improvement in the quality of the tomogram when the background of the tilt series is optimised (Fig. 4d, right). Using surface rendering, Fig. 4g and h compares the differences in quality of the segmentation of the tomograms for separating the Au cores from the Ag shells using the intensity ranges shown in brackets in Fig. 4b. In the case of the tomogram using a tilt series with the optimised background, there is no gap between the two ranges of intensities used for the segmentation. Comparing Fig. 4e with the image at 0° tilt in Fig. 4a, background optimisation permits a more faithful segmentation/visualisation in terms of the sizes and shapes of the Ag particles and the Au cores. This is a clear indication that the reconstruction improves, because less blurring also implies a better separation of intensity ranges corresponding to distinct materials or phases present in the specimen.

Supplementary material related to this article can be found online at doi:10.1016/j.ultramic.2015.03.017.

4.3. BF TEM tomography: improvement of resolution.

BF TEM is normally used for ET of amorphous and soft materials, which is typically the case of biological samples [21,41]. Fig. 5a shows a BF TEM image acquired at 0° tilt of a powder of Vulcan XC-72R, a commercial carbon black that find applications in heterogeneous catalysis and that lacks long-range order [19,20,42]. For tomographic reconstruction, the intensities of the tilt series were inverted ($I_{x,y} \rightarrow -I_{x,y}$), as shown in Fig. 5b, because it facilitates further segmentation of the tomogram although this step is not necessary in general. The minimum intensity value of the inverted series is found to be the value −5060, which is greater than the absolute minimum of −32,678 for the image format used in our experiments. Hence, background optimisation of the BF TEM tilt series is a critical step in order to reconstruct better tomograms to compensate for the resulting offset of the vacuum level. The correction is applied by downshifting the intensities by an amount of 27,618 that is the difference between −32,678 and −5060. Fig. 5c shows a model of carbon black made of a tortuous 3D aggregation of spherical nanocrystallites. Fig. 5d and e are the voltex visualisation of the tomograms with and without background optimisation of the tilt series. As in the case of HAADF STEM tomography. Fig. 5f is the same as Fig. 5d but with the visualisation optimised in the range [−1678, 1000] to remove the effect of the blurring. In the case of the voltex visualisation of the tomogram obtained using the optimised tilt series, only was

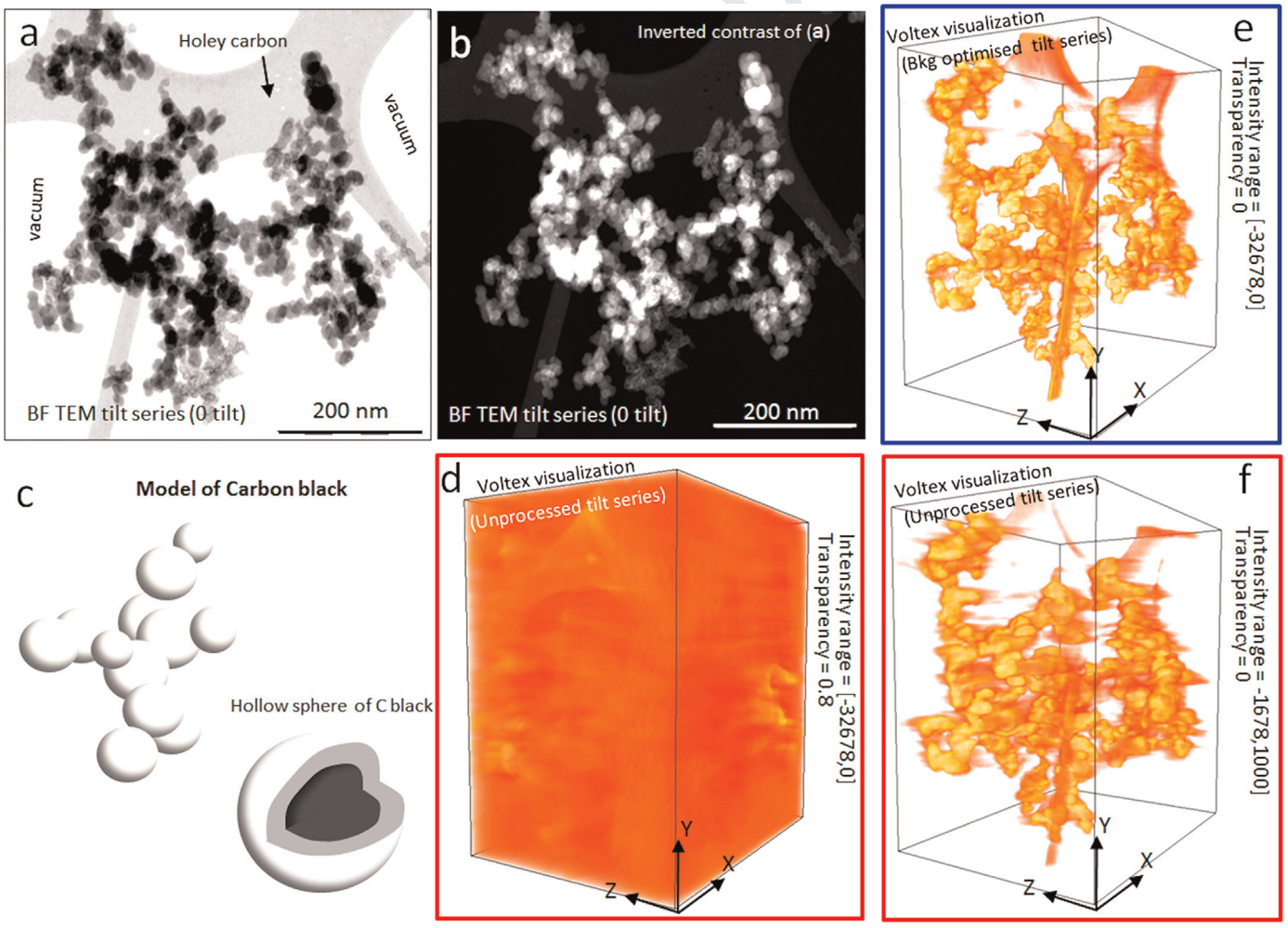

Fig. 5. Background optimisation in BF TEM tomography. (a) Representative image from a tomographic tilt series of 71 images of a powder of carbon black deposited on an amorphous holey carbon film and acquired in the angular range between −70° and +70° with a step of 2°. The intensity of the vacuum in (a) is not saturated (I_{vaccum} = 5060 < saturation value = +32,677). (b) Inverted version of (a) for tomographic reconstruction. (c) Model of carbon black as a 3D aggregation of hollow spheres with concentric layers of carbon. (d) Three-dimensional visualisation of the tomogram of the sample. (f) In order to remove the cloud of intensity in the vacuum that obscures the sample, it was necessary to adjust the intensity range to [−1678, 1000]. (e) Three-dimensional visualisation of the tomogram of the sample obtained using the tilt series with the background optimised. (Video S3 supporting info).

Please cite this article as: L.C. Gontard, Removing the effects of the "dark matter" in tomography, Ultramicroscopy (2015), http://dx.doi.org/10.1016/j.ultramic.2015.03.017

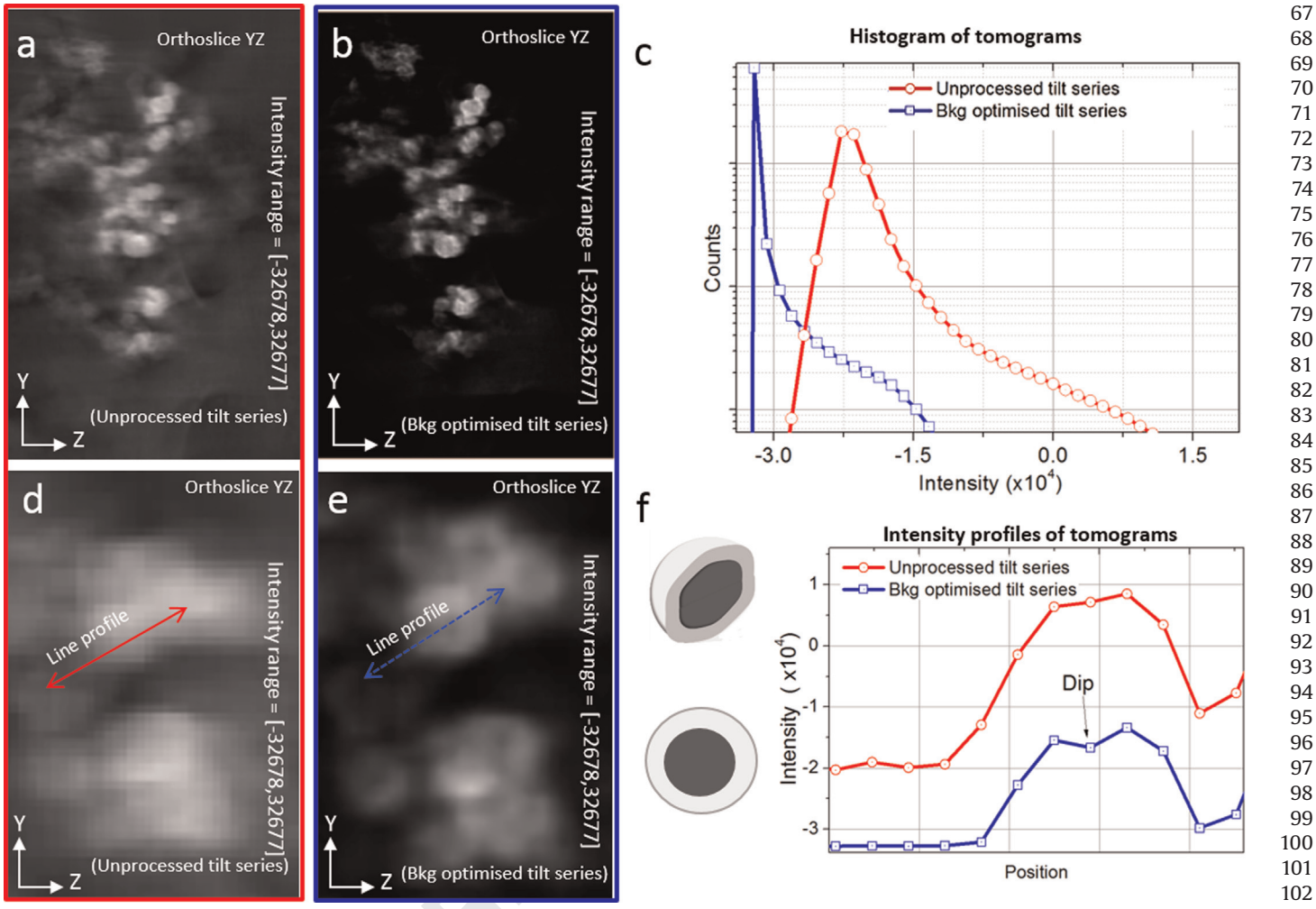

Fig. 6. Improvement of resolution in background-optimised BF-TEM tomography. (a) ZY othoslice of the tomogram obtained using the unprocessed tilt series shown in Fig. 4. (b) The same orthoslice from the tomogram calculated from the background-optimised tilt series. (c) Histograms of the two tomograms. (d) and (e) are details of the fidelity of the reconstructed nanocrystallites. When the background is optimised, blurring largely disappears in ZY orthoslices and the hollow centres of the carbon spheres are clearly recognised. (f) Intensity profiles measured along the line profiles indicated in (d) and (e) with arrowed lines. When the background is optimised, the orthoslices of the tomogram correctly show the bright ring structure expected from a hollow sphere.

necessary to set the upper range to 0 for display purposes. Comparing Fig. 5e and f it is clear that when the tilt series is optimised the carbon film and the carbon black are better separated and there is less blurring in the *z*-direction.

The spherical crystallites in most commercial carbon blacks have an average of approximately four graphite concentric layers with a hollow centre [42]. Fig. 6a and b compares YZ orthoslices of the tomograms of the carbon black specimen using the unprocessed tilt series with the background optimised. In this case, artefacts are absent to a great extent, and details are clearly enhanced (spatial resolution improves). This is most evident in Fig. 6e, in which the crystallites show a bright rim with a dark centre, as one would expect for the hollow sphere crystallites of this carbon black.

5. Conclusion

In general, an absolute reference level of intensities is not available in ET unless an area of the sample in vacuum is exposed. If the minimum level of intensity of a tilt series that correspond with a real phase of the material is not adjusted so that it coincides with the absolute minimum value of the dynamic range of the electron detector system (or of the image format used), the tomogram will display typically intensities in places which should correspond to vacuum. These intensities will blur the full volume and will enhance the artefacts introduced by the MW. In such cases, the fidelity of a tomogram obtained using iterative reconstruction methods can be greatly improved (with more contrast, fewer artefacts, and better accuracy) easily if the background level of the tilt series is downshifted before its reconstruction. Moreover, this step facilitates further segmentation and visualisation of the three-dimensional tomogram. We believe that this type of preprocessing should always be performed in order to obtain optimal results irrespective of the imaging technique used. It is also complementary with the use of other methodologies for minimising the MW effects. And we envisage that this simple methodology can be also an effective way of thresholding an embedding material or a low-density supporting thin film that are not part of the sample under examination but that are typically used for sample preparation of biological samples or as supports of nanostructures respectively.

Supporting information

- Three videos S1–S3 showing the visualisation of the tomograms before and after background processing.

Please cite this article as: L.C. Gontard, Removing the effects of the "dark matter" in tomography, Ultramicroscopy (2015), http://dx.doi.org/10.1016/j.ultramic.2015.03.017

- A programme of software written in Matlab for performing background optimisation of.mrc files for tomographic reconstruction using FEI software is available at www.lcgontard.es. The file called *BKG_Optimisation_Tomography_LCG_2015.exe* is an executable and therefore it requires the preinstallation of Matlab MCR above version 2012b.

Acknowledgements

The author wishes to thank different collaborators that provided the samples or support, Prof. Rafal E Dunin-Borkowski, Dr. Ana Becerro, Dr. Dogan Ozkaya and Dr. Cuong Cao. The author is also grateful to Prof. Asunción Fernández as leader of the European Project REGPOT-CTAl-NANOFUNC and to the European Union under a Contract for an Integrated Infrastructure Initiative 312483-ESTEEM2 for funding.

References

[1] R.A. Crowther, D.J. de Rosier, A. Klug., The reconstruction of a three-dimensional structure from projections and its application to electron microscopy, Proc. R. Soc. Lond. A 319 (1970) 317–340.
[2] A.J. Koster, U. Ziese, A.J. Verkleij, A.H. Janssen, K.P. de Jong, Three-dimensional transmission electron microscopy: a novel imaging and characterization technique with nanometer scale resolution for materials science, J. Phys. Chem. B 104 (2000) 9368–9370.
[3] M. Weyland. Two and Three-dimensional Nanoscale Analysis: New Techniques and Applications (Ph.D. thesis), University of Cambridge, 2002.
[4] P.A. Midgley, R.E. Dunin-Borkowski, Electron tomography and holography in materials science, Nat. Mater. 8 (2013) 271–280.
[5] P.R. Buseck, R.E. Dunin-Borkowski, B. Devouard, R.B. Frankel, M.R. McCartney, P.A. Midgley, M. Pósfai, M. Weyland, Magnetite morphology and life on Mars, Proc. Natl. Acad. Sci. 98 (24) (2001) 13490–13495.
[6] M. Weyland, Electron tomography of catalysts, Top. Catal. 21 (4) (2002) 175–183.
[7] T.J.V. Yates, The development of electron tomography for nanoscale materials science applications (Ph.D. thesis), University of Cambridge, 2005.
[8] H. Friedrich, P.E. de Jongh, A.J. Verkleij, K.P. de Jong, Electron tomography for heterogeneous catalysts and related nanostructured material, Chem. Rev. 109 (5) (2009) 1613–1629.
[9] G. Möbus, R.C. Doole, B.J. Inkson, Spectroscopic electron tomography, Ultramicroscopy 96 (2003) 433–451 (3–4).
[10] P. Ercius, M. Weyland, D.A. Muller, L.M. Gignac, Three-dimensional imaging of nanovoids in copper interconnects using incoherent bright field tomography, Appl. Phys. Lett. 88 (2006) 243116.
[11] A. Yurtsever, M. Weyland, D.A. Muller., Three-dimensional imaging of nonspherical silicon nanoparticles embedded in silicon oxide by plasmon tomography, Appl. Phys. Lett. 89 (2006) 151920.
[12] M. Weyland, P.A. Midgley, Extending energy-filtered transmission electron microscopy (EFTEM) into three-dimensions using electron tomography, Microsc. Microanal. 9 (2003) 542–555.
[13] M.H. Gass, K.K.K. Koziol, A.H. Windle, P.A. Midgley, 4-dimensional spectral-tomography of carbonaceous nano-composites, Nano Lett. 6 (2006) 376–379.
[14] L.C. Gontard, J.R. Jinschek, H. Ou, J. Verbeeck, R.E. Dunin-Borkowski, Three-dimensional fabrication and characterisation of core-shell nanocolumns using electron beam patterning of Ge-doped SiO_2, Appl. Phys. Lett. 100 (2012) 263113.
[15] M.C. Scott, C.C. Chen, M. Mecklenburg, C. Zhu, R. Xu, P. Ercius, U. Dahmen, B. C. Regan, J. Miao, Electron tomography at 2.4-Å resolution, Nature 483 (2012) 444–448.
[16] B. Goris, L. Polavarapu, S. Bals, G. Van Tendeloo, L.M. Liz-Marzá, Monitoring galvanic replacement through three-dimensional morphological and chemical mapping, Nano Lett. 14 (2014) 3220–3226.
[17] N. Volkmann, Chapter two-methods for segmentation and interpretation of electron tomographic reconstructions, Method. Enzymol 483 (2010) 31–46.
[18] S. Lozano-Pérez, P. Rodrigo, L.C. Gontard, Three-dimensional characterization of stress corrosion cracks, J. Nucl. Mater. 408 (2011) 289–295.
[19] L.C. Gontard, R.E. Dunin-Borkowski, D. Ozkaya, Three-dimensional shapes and spatial distributions of Pt and PtCr catalyst nanoparticles on carbon black, J Microsc. 232 (2) (2008) 248–259.
[20] L.C. Gontard, R.E. Dunin-Borkowski, M.H. Gass, A.L. Bleloch, D. Ozkaya, Three-dimensional shapes and structures of lamellar-twinned fcc nanoparticles using ADF STEM, J. Electron Microsc. 58 (2009) 167–174.
[21] L.C. Gontard, B.R. Knappett, A.E.H. Wheatley, S.L.-Y. Chang, A. Fernández, Impregnation of carbon black for the examination of colloids using TEM, Carbon 76 (2014) 464.
[22] J.R. Tong, I. Arslan, P.A. Midgley, A novel dual-axis iterative algorithm for electron tomography, J. Struct. Biol. 153 (1) (2006) 55–63.
[23] J.J. Fernández, C.O.S. Sorzano, R. Marabini, J.M. Carazo, Image processing and 3-D reconstruction in electron microscopy, IEEE Signal Process. Mag. 23 (3) (2006) 84–94.
[24] J.-J. Fernández, Computational methods for materials characterization by electron tomography, Curr. Opin. Solid State Mater. Sci. 17 (2013) 93–105.
[25] M. Cao, H.-B. Zhang, Y. Lu, R. Nishi, A. Takaoka, Formation and reduction of streak artefacts in electron tomography, J. Microsc. 239 (1) (2010) 66–71.
[26] V. Ortalan, M. Herrera, D.G. Morgan, N.D. Browning, Application of image processing to STEM tomography of low-contrast materials, Ultramicroscopy 110 (2009) 67–81.
[27] T. Roelandts, K.J. Batenburg, E. Biermans, C. Kübel, S. Bals, J. Sijbers, Accurate segmentation of dense nanoparticles by partially discrete electron tomography, Ultramicroscopy 114 (2012) 96–105.
[28] A. Lange, A. Kupsch, M.P. Hentschel, I. Manke, N. Kardjilov, T. Arlt, R. Grothausmann, Reconstruction of limited computed tomography data of fuel cell components using direct iterative reconstruction of computed tomography trajectories, J. Power Sources 196 (2011) 5293–5298.
[29] A. Alpers, R.J. Gardner, S. König, R.S. Pennington, C.B. Boothroyd, L. Houben, R. E. Dunin-Borkowski, K.J. Batenburg, Geometric reconstruction methods for electron tomography, Ultramicroscopy 128 (2013) 42–54.
[30] B. Goris, W. Van den Broek, K.J. Batenburg, H.H. Mezerji, S. Bals, Electron tomography based on a total variation minimization reconstruction technique, Ultramicroscopy 113 (2012) 120–130.
[31] R. Leary, Z. Saghi, P.A. Midgley, D.J. Holland, Compressed sensing electron tomography, Ultramicroscopy 131 (2013) 70–91.
[32] A. Frangakis, R. Hegerl, Noise reduction in electron tomographic reconstructions using nonlinear anisotropic diffusion, J. Struct. Biol. 135 (2001) 239–250.
[33] J.J. Fernández, S. Li, An improved algorithm for anisotropic nonlinear diffusion for denoising cryo-tomograms, J. Struct. Biol. 144 (2003) 152–161.
[34] C.J. Gommes, K. de Jong, J.-P. Pirard, S. Blacher, Assessment of the 3D localization of metallic nanoparticles in Pd/SiO_2 cogelled catalysts by electron tomography, Langmuir 21 (2005) 12378–12385.
[35] R. Grothausmann, G. Zehl, I. Manke, S. Fiechter, P. Bogdanoff, I. Dorbandt, A. Kupsch, A. Lange, M.P. Hentschel, G. Schumacher, J. Banhart, Quantitative structural assessment of heterogeneous catalysts by electron tomography, J. Am. Chem. Soc. 133 (2011) 18161–18171.
[36] G.T. Herman, Image Reconstruction from Projections: Implementation and Applications, Topics in Applied Physics, 32, Springer-Verlag, 1979.
[37] C. Yang, H. Zhang, J. Li, A. Takaoka, The top-bottom effect of a tilted thick specimen and its influence on electron tomography, J. Electron Microsc. 54 (4) (2005) 367–371.
[38] A.I. Becerro, J. Criado, L.C. Gontard, S. Obregón, A. Fernández, G. Colón, M. Ocaña, Bifunctional, monodisperse $BiPO_4$-based nanostars: photocatalytic activity and luminescent applications, Cryst. Growth Des. 14 (2014) 3319–3326.
[39] A. Martinez-Sanchez, I. Garcia, J.J. Fernandez, A differential structure approach to membrane segmentation in electron tomography, J. Struct. Biol. 175 (2011) 372–383.
[40] C. Cao, L.C. Gontard, L.L.T. Tram, A. Wolff, D.D. Bang, Dual enlargement of gold nanoparticles: from mechanism to scanometric detection of pathogenic bacteria, Small 7 (12) (2011) 1701–1708.
[41] R. Grimm, H. Singh, R. Rachel, D. Typke, W. Zillig, W. Baumeister, Electron tomography of ice-embedded prokaryotic cells, Biophys. J. 74 (1998) 1031.
[42] R.D. Heidenreich, W.M. Hess, L.L.A. Ban, A test object and criteria for high resolution electron microscopy, J. Appl. Cryst. 1 (1968) 1–19.

Please cite this article as: L.C. Gontard, Removing the effects of the "dark matter" in tomography, Ultramicroscopy (2015), http://dx.doi.org/10.1016/j.ultramic.2015.03.017